Engineering Structures 280 (2023) 115640

Contents lists available at ScienceDirect

Engineering Structures

journal homepage: www.elsevier.com/locate/engstruct

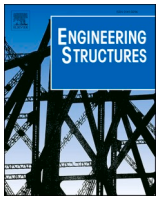

A steel bracing system dissipating energy through moment-rotation hysteresis loops

Alessandro Mei, Federico Gusella, Maurizio Orlando *

University of Florence, Department of Civil and Environmental Engineering, Italy

ARTICLE INFO

Keywords:
Capacity design
Experimental tests
Rotation ductility
Non-linear behavior
Energy dissipation
Steel bracing system

ABSTRACT

According to the capacity design method, earthquake-resistant structures should be able to dissipate energy through dissipative regions, which are expected to yield while the other structural members remain in the elastic field during seismic excitation. The non-linear response of a bracing system, in which energy dissipation relies on a fuse, is investigated through experimental tests and numerical analyses. Loading on the fuse is a combination of bending moment, axial, and shear load. Results provide valuable information on the influence of several design parameters, such as the member cross-section compactness, shape, and member slenderness. The stability of the moment-rotation hysteresis loops and the energy dissipation are assessed through cyclic tests.

To promote the utilization of the proposed bracing system in earthquake resistant steel structures, the work concludes by highlighting that the fuses are easily replaceable while ensuring ductile system response.

1. Introduction

Earthquake-resistant structures, designed according to the capacity design requirement, require the ability to dissipate energy through dissipative regions, which are expected to yield under seismic actions [1], while brittle failures are avoided. Several systems capable of dissipating energy through plastic deformations have been experimentally investigated: semi-rigid beam-to-column connections of moment resisting frame in [2–9]; cold-formed steel elements in [10–16]; shear walls in [17–19] checking the bolts to be characterized by overstrength [20] and diagonals of concentric X bracing systems formed by hot-rolled members in [21–24]. Several studies have been developed in increasing the ductility and dissipation of energy of concentric bracing systems equipped with devices, particular shapes, and materials.

In [25], hybrid braced frames with buckling-restrained strong braces to mitigate soft story are investigated. In [26], a yielding octagonal connection for concentrically braced frames is proposed and numerically investigated. In [27], the hysteresis curve of braced frame structures is largely increased, equipping diagonals with a double-cylinder as an energy dissipator. Innovative passive shear dampers are designed and tested in [28–30]. Experimental tests on scale braced frames with replaceable brace modules and bolted unstiffened connections are carried out in [31]. The introduction of dissipative floor connectors is assessed in [32]. U-shaped steel plates to join diagonals to columns are adopted in [33]. The seismic risk of braces in existing concentrically braced frame buildings designed according to previous and current seismic provisions is addressed in [34]. The effectiveness of staggered braces in reducing the load on vertical members and foundations is investigated in [35]. The capacity to increase the ductility of concentrically braced frames through the plastic deformation capacity of channel-encased braces is investigated in [36]. In [37] to promote the yielding of existing diagonal braces in concentric X-bracing systems, the diagonal material strength is reduced through thermal treatment.

One of the most critical issues that researchers are faced is the reduction of the extensive damage and permanent deformations in the structures after earthquakes. In [38], an experimental study of new axial recentering dampers equipped with shape memory alloy plates is conducted to solve this problem. In [39,40] self-centering concentrically braced frames are analyzed.

Another important aspect related to concentric bracing systems under study by researchers is to satisfy the capacity design requirements calibrating the yielding diagonal resistance, leaving the brace slenderness practically unchanged. For this purpose, concentrically braced frames with reduced sections for bracing members or equipped with additional holes are proposed in [41,15].

The main feature of the investigated knee-braced frame is the capacity to dissipate energy in a plastic mechanism satisfying the code requirements and being easily replaceable after a seismic event.

* Corresponding author at: University of Florence, Dipartimento di Ingegneria Civile e Ambientale, Via di S. Marta 3, 50139 Firenze, Italy.
E-mail addresses: alessandro.mei@unifi.it (A. Mei), federico.gusella@unifi.it (F. Gusella), maurizio.orlando@unifi.it (M. Orlando).

https://doi.org/10.1016/j.engstruct.2023.115640
Received 8 October 2022; Received in revised form 24 December 2022; Accepted 12 January 2023
Available online 26 January 2023

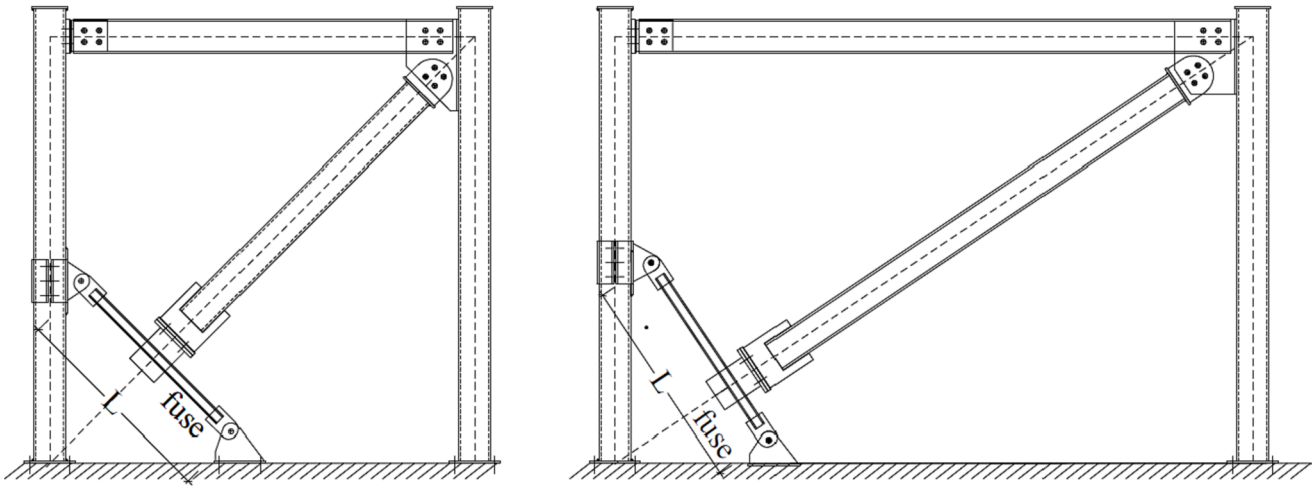

Fig. 1. Proposed bracing system for square or rectangular bay with identification of the fuse.

Table 1

Geometrical parameters of the fuse (UPN – RHS)

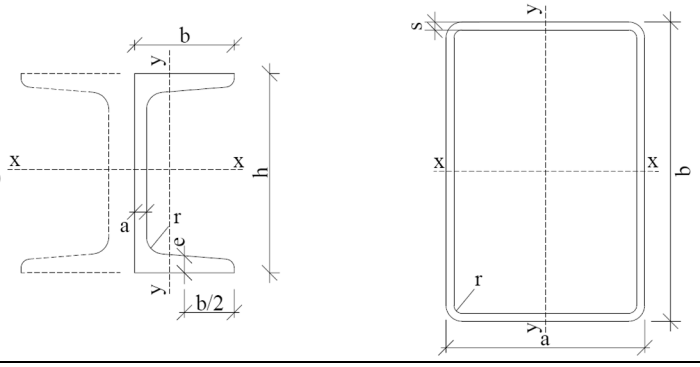

Single channel section - UPN										
h [mm]	b [mm]	a [mm]	e [mm]	r [mm]	Weight [kg/m]	Cross-section area [cm^2]	Second moment of area		Section modulus	
							J_{xx} [cm^4]	J_{yy} [cm^4]	$W_{e,xx}$ [cm^3]	$W_{p,xx}$ [cm^3]
50	38	5	7	7	5.6	7.1	26.5	9.1	10.1	13.0
100	50	6	8.5	8.5	10.6	13.5	205.0	29.1	41.1	49.0

Rectangular hollow section – RHS								
Shape b x a	s [mm]	Weight [kg/m]	Cross-section area [cm^2]	Second moment of area		Section modulus	
				J_{xx} [cm^4]	J_{yy} [cm^4]	$W_{e,xx}$ [cm^3]	$W_{p,xx}$ [cm^3]
80x40	5	8.4	10.7	80.1	25.6	20.0	26.1
150x100	4	15.2	19.4	617.3	328.6	82.3	97.4

Table 2
Mechanical properties of steel from coupon tests.

Member	f_y [N/mm^2]	f_u [N/mm^2]	$\Delta = \frac{L_f - L_i}{L_i}$ [%] (1)	Steel Grade
UPN50	352	472	35.8	S275
UPN100	322	451	34.9	S275
80x40x5	381	432	28.5	S235
150x100x4	340	465	35.2	S235

(1) L_f and L_i are the final length at fracture and the initial length of the specimen used in the coupon test, respectively.

The investigated bracing system (Fig. 1) has a transverse beam that behaves like a fuse and is designed against out-of-plane buckling. The long diagonal is a truss under tension and compression, which under seismic actions does not buckle, remains in the elastic field, and transfers a concentrated load to the fuse, which is subjected to a three-point bending load and dissipates energy through moment-rotation hysteresis loops.

Preliminary studies into the behavior of knee-braced frames subjected to seismic loading are performed in [42] where the non-linear response of the proposed bracing system is compared to that of eccentric bracing systems. In [43], the importance of preventing the buckling of the fuse is highlighted, and all studies highlighted the high energy dissipation capacity of the system during severe lateral loads. In [44], a knee-braced frame with a shear-yielding knee is investigated. Experimental results reveal that when the knee is designed with a web stiffener to prevent tearing of the web, it can dissipate a large amount of energy during an earthquake.

The seismic behavior of knee-braced steel frames is investigated in [45,46] performing incremental dynamic analyses and providing information about the influence on the elastic stiffness, ductility, and

Table 3

Classification of the fuse cross-section

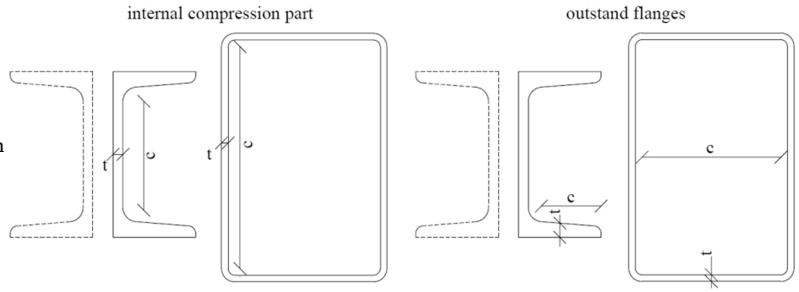

Specimen	Cross-section	f_{yk} [N/mm^2]	ε	c/t	Compression part	Class(*)
UPN_{50}	UPN 50x38	275	0.92	4.4	Internal compression part	1
				3.71	Outstand flanges	1
UPN_{100}	UPN 100x50	275	0.92	11	Internal compression part	1
				4.18	Outstand flanges	1
RHS_{80}	80x40x5	235	1	12	Lateral Internal compression part	1
				4	Flange Internal compression part	1
RHS_{150}	150x100x4	235	1	33.5	Lateral Internal compression part	1
				21	Flange Internal compression part	1

(*) for internal compression part: 1st class, $c/t \leq 72\varepsilon$; 2nd class, $72\varepsilon < c/t \leq 83\varepsilon$ and 3th class, $83\varepsilon < c/t \leq 124\varepsilon$; for outstand flanges: 1st class, $c/t \leq 9\varepsilon$, 2nd class, $9\varepsilon < c/t \leq 10\varepsilon$ and 3th class, $10\varepsilon < c/t \leq 14\varepsilon$ [51]; with $\varepsilon = \sqrt{235/f_{y,k}}$.

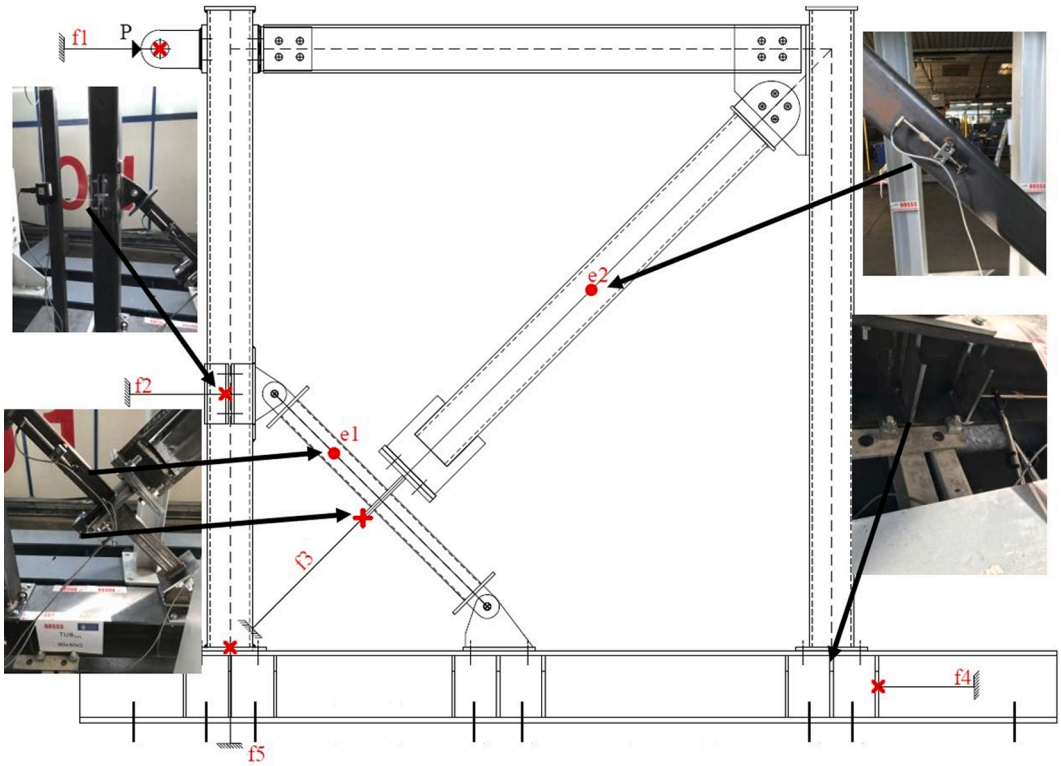

Fig. 2. Instrumentation layout: wire-actuated encoders (f_1-f_5) and omega strain gages (e_1-e_2).

probability of failure of these systems due to several design parameters such as the length of the knee and the number of stories.

In [47], a numerical comparison in adopting knee-braced moment frames using pinned and rigid connections is performed. Fixed connections to join the fuse to the frame are recommended to increase the system's stiffness and energy dissipation.

A small-scale dynamic model of a building with knee-braced steel frames is developed in [48], proving to be appropriate in investigating the response of a true-scale building.

In [49], the structural response of a system where energy dissipation is provided by a knee-bracing frame and a friction damper with long slotted holes is investigated.

In [50], a reduction factor of 5.63 and an equivalent damping ratio of 23 % is estimated for knee-braced frames.

If the capacity of the fuse to dissipate, energy undergoing plastic deformation is well recognized; its replacement after a seismic is a topic that requires analysis and is investigated in the present paper.

The main features of the proposed system are the vast customization and applicability in earthquake-resistant steel structures designed according to the capacity design. The bracing system is capable of ensuring

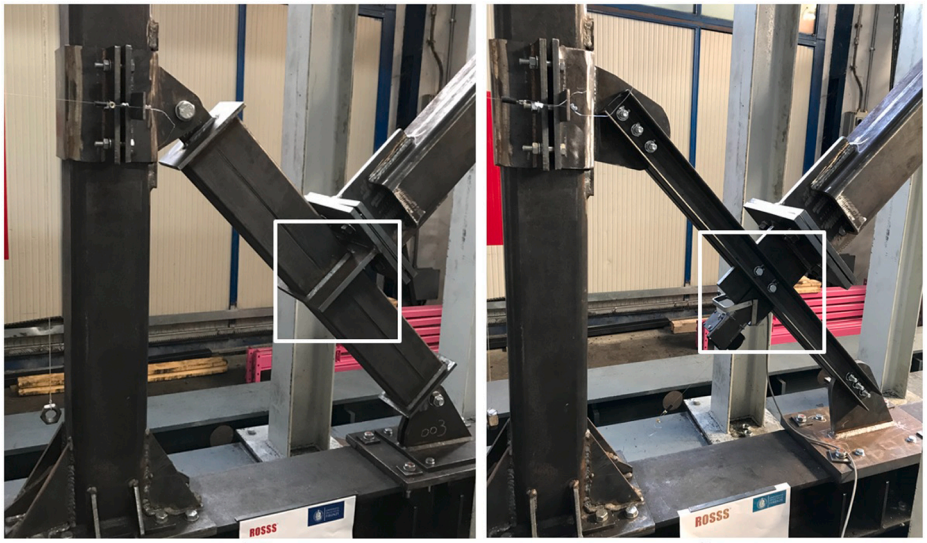

a) b)

Fig. 3. Types of connection between the fuse and the long diagonal. a) RHS_{150}, b) UPN_{50}.

Table 4
List of experimental tests.

Specimen	Cross-section	Loading History	Connection at fuse mid span	Connection at fuse-ends
UPN_{50m}	2xUPN50	monotonic	2 M12	3 M12
UPN_{50c}	2x UPN50	cyclic	2 M12	3 M12
RHS_{80m}	RHS80x40x5	monotonic	welded	1 M22
RHS_{80c}	RHS80x40x5	cyclic	welded	1 M22
UPN_{100m}	2x UPN100	monotonic	2 M22	1 M22
UPN_{100c}	2x UPN100	cyclic	2 M22	1 M22
RHS_{150m}	RHS150x100x4	monotonic	welded	1 M22
RHS_{150c}	RHS150x100x4	cyclic	welded	1 M22

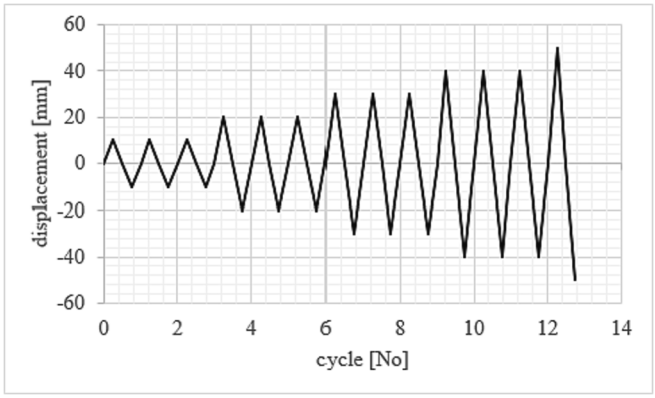

Fig. 4. Loading history of cyclic tests as per ATC-24 [56].

a stable, satisfactory behavior under cyclic load and is efficiently designed to promote a homogeneous dissipative behavior in tall structures.

These considerations highlight the proposed bracing system as an alternative to the classic X bracing system for earthquake-resistant steel structures designed according to the capacity design approach.

In concentric X bracing systems, the seismic energy is dissipated by diagonals through force–elongation hysteresis loops. The diagonal plastic resistance depends on the cross-section area and the steel yield strength; the elongation only depends on the member length, the steel yield strength, and the steel modulus of elasticity [51]. In the proposed bracing system, more parameters can be easily changed according to the design requirements, highlighting its broad applicability. In particular, the resistance is related to the fuse yield moment $M_y = f_y W_{xx}$ (with W_{xx} the elastic section modulus and f_y the steel yield strength); the plastic elongation in the long diagonal axis direction depends on the fuse flexural deformation and then on the fuse yield moment, the fuse length L, and the second moment of area J of the fuse cross-section. The energy dissipation is given by stable moment-rotation hysteresis loops, which are more significant than those provided by force–elongation cycles [52].

In X-bracing systems, compressed diagonal braces buckle under seismic action and are usually seriously damaged after an earthquake, so their replacement is hard. In the proposed bracing system, the fuse is the only member undergoing plastic deformation, and when it is joined to the portal frame by a single bolt, its replacement is straightforward.

Finally, unlike eccentric bracings, the beam of the portal frame, which usually bears the live load, is designed to remain in an elastic field. Its damage is avoided without reducing or interrupting the structure's logistic flows.

Results of experimental tests of the full-scale bracing system are presented. Tests involve several profiles with different structural details, geometrical features, and mechanical properties. A Finite Element (FE) numerical model, checked by comparison with numerical results, is developed and adopted to highlight the influence on the bracing system structural response of the cross-section compactness and slenderness of the fuse. An analysis of the stress distribution is performed, confirming the fuse to be the only element to undergo plastic deformation. The fuses enable expedient repair after a seismic event while ensuring ductile system response. The paper concludes by estimating the seismic behavior factor of the investigated bracing system promoting its application.

2. Experimental campaign

2.1. Geometry of specimens

The paper compares the structural response of the same bracing system in which only the fuse is changed. Fuses belong to the same class [53] but have a different cross-section shape and connection details (Table 1). Double channel sections (UPN) have about the same elastic section modulus ($W_{e,xx}$) around the strong x-axis of rectangular hollow sections (RHS). All fuse cross-sections are designed to prevent out-of-

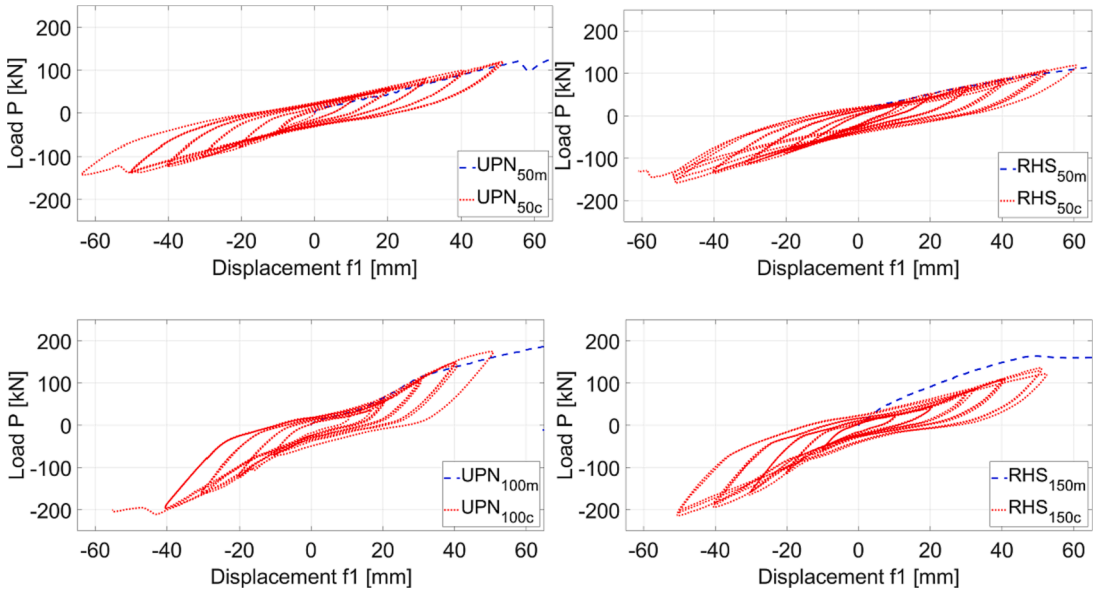

Fig. 5. Monotonic and cyclic curves (P-f_1). Tests UPN_{50}, RHS_{50}, UPN_{100}, RHS_{150}.

Table 5
List of the failure modes of all specimens and absolute value of the maximum experimental load achieved in cyclic tests.

Specimen	Failure mode	|Pmax| [kN] in cyclic tests
UPN_{50m}	local buckling	138 (UPN_{50c})
UPN_{50c}	local buckling – failure of oustand flanges	
RHS_{80m}	local buckling – weld failure	148 (RHS_{80c})
RHS_{80c}	local buckling – weld failure	
UPN_{100m}	local buckling	210 (UPN_{100c})
UPN_{100c}	local buckling – failure of oustand flanges	
RHS_{150m}	local buckling	214 (RHS_{150c})
RHS_{150c}	local buckling – failure of oustand flanges	

plane instability and allow the formation of a plastic hinge which dissipates energy during earthquake. The response of different fuse cross-sections was characterized through a preliminary experimental campaign of the fuse alone in three-point bending [54]. The columns, the long diagonal and the upper beam are designed as over-strength members and have a rectangular hollow section (150x150x10). The bracing system bay is 2000 mm long and 2000 mm high. The fuse length is $L = 1000$ mm (Fig. 1).

Table 2 gives the experimental yield strength f_y, the ultimate strength f_u, the percentage total elongation at failure (Δ) and the steel grade for each specimen. All experimental values (f_y, f_u and Δ) represent the average values of three coupon tests according to [55] on the steel coil used to manufacture specimens. Table 3 gives the characteristic yield strength f_{yk}, the ratio c/t and the section class of the the fuse cross-section according to [53].

2.2. Test set-up and loading protocol

Bracing systems are investigated through experimental tests. The testing apparatus is shown in Fig. 2, fuses are 1000 mm long (distance between pinned member-ends – one bolt M22 grade 8.8 [53]. Tests are conducted under load control until failure. For each specimen, monotonic and cyclic tests are performed. The horizontal load (P) is applied at the top of the frame, and it is measured through a load cell. The horizontal displacement at the loaded section is monitored directly by the linear variable displacement transducer of the testing machine (f_1). The eventually horizontal and vertical displacement of the testing frame, due to the sliding of nuts in connections with bolts, is monitored by wire-actuated encoders f_4 and f_5, respectively. The displacement at the fuse mid span, in the direction of the load application, by f_3, the horizontal displacement at the fuse-column connection by f_2. Omega strain gauges

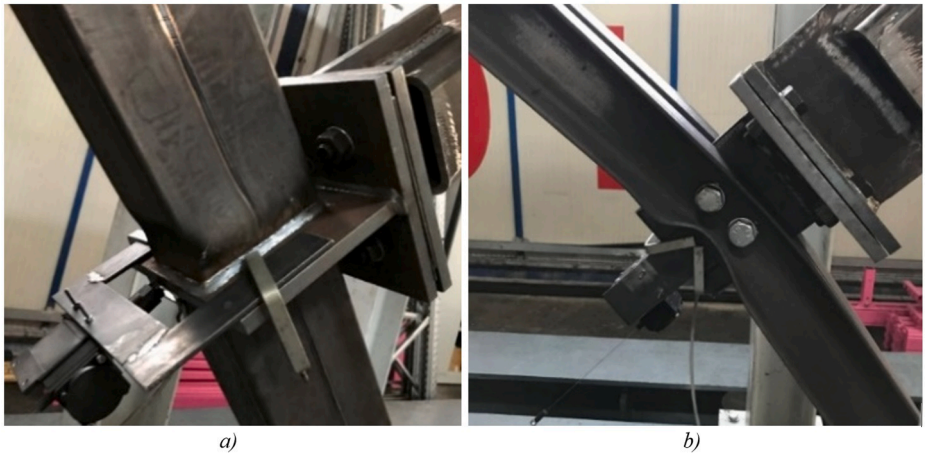

a) *b)*

Fig. 6. Failure modes observed in experimental tests. a) RHS_{150c} - local buckling b) UPN_{100c} - local buckling.

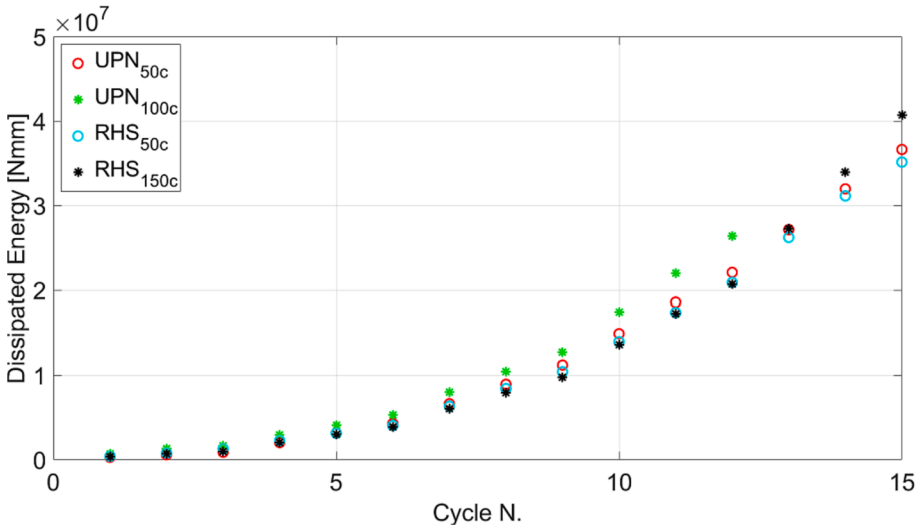

Fig. 7. Dissipated energy versus number of cycles.

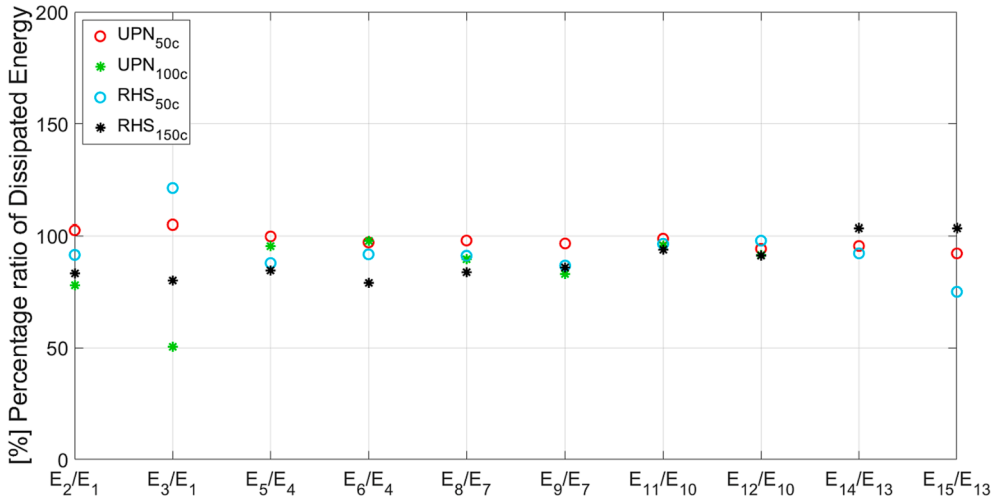

Fig. 8. Degradation of the energy dissipation capacity in the second and third cycle of each three-cycle series relative to the first cycle.

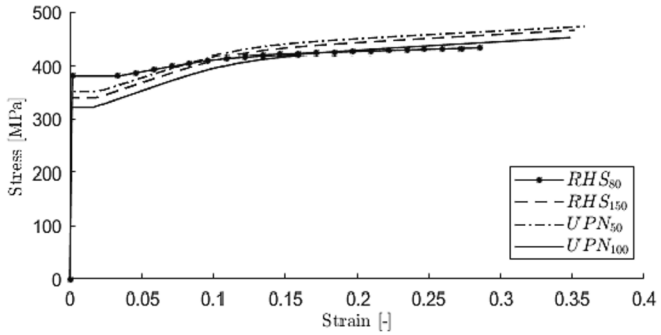

Fig. 9. Steel constitutive law used for each specimen.

(e_1 and e_2) are placed at L/2 of the diagonal and L/4 from support of the fuse (Fig. 2). The connections between the fuse and the bracing frame are design as overstrength joint (Fig. 3). UPN specimens are connected to the diagonal element through bolts (Fig. 3a). Profiles with a rectangular hollow section (RHS) are connected by welds (Fig. 3b). Bolted connections are adopted to join the fuse to the frame.

The loading protocol is shown in Table 4. Double channel sections and rectangular hollow sections are named $UPN_{\alpha\beta}$ and $RHS_{\alpha\beta}$, respectively, where α identifies the height of the fuse cross-section and β = m means that a monotonic load is applied, β = c a cyclic load.

Table 6
Properties for the cyclic isotropic-kinematic model used in the FEA (according to [60]).

	Initial yield stress	Isotropic hardening magnitude for cyclic hardening	Isotropic hardening rate parameter for cyclic hardening
	$\sigma_{y,0}$	Q_∞	b
RHS_{80}	381.45	138.01	11.36
RHS_{150}	340.30	138.01	11.36
UPN_{50}	352.40	138.01	11.36
UPN_{100}	322.51	138.01	11.36

2.3. Displacement history

Monotonic and cyclic tests are interrupted at the fuse failure. The cyclic response of bracing system is investigated under the cyclic displacement history illustrated in Fig. 4. A quasi-static cyclic loading is applied per ATC-24 loading protocol [56]. A symmetric three-cycle

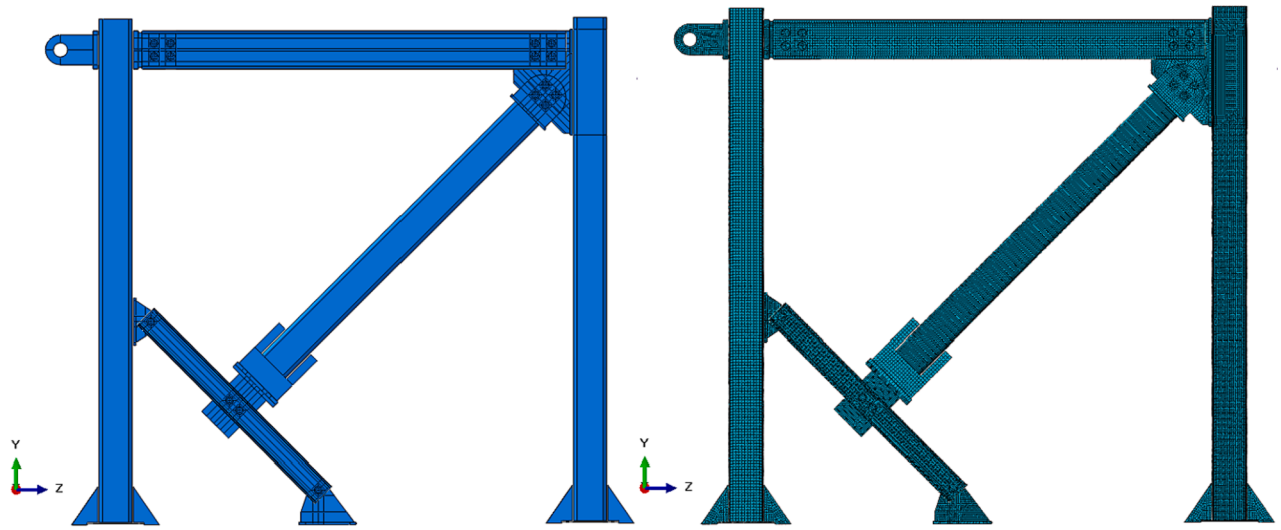

Fig. 10. FE model: geometry (left); mesh (right).

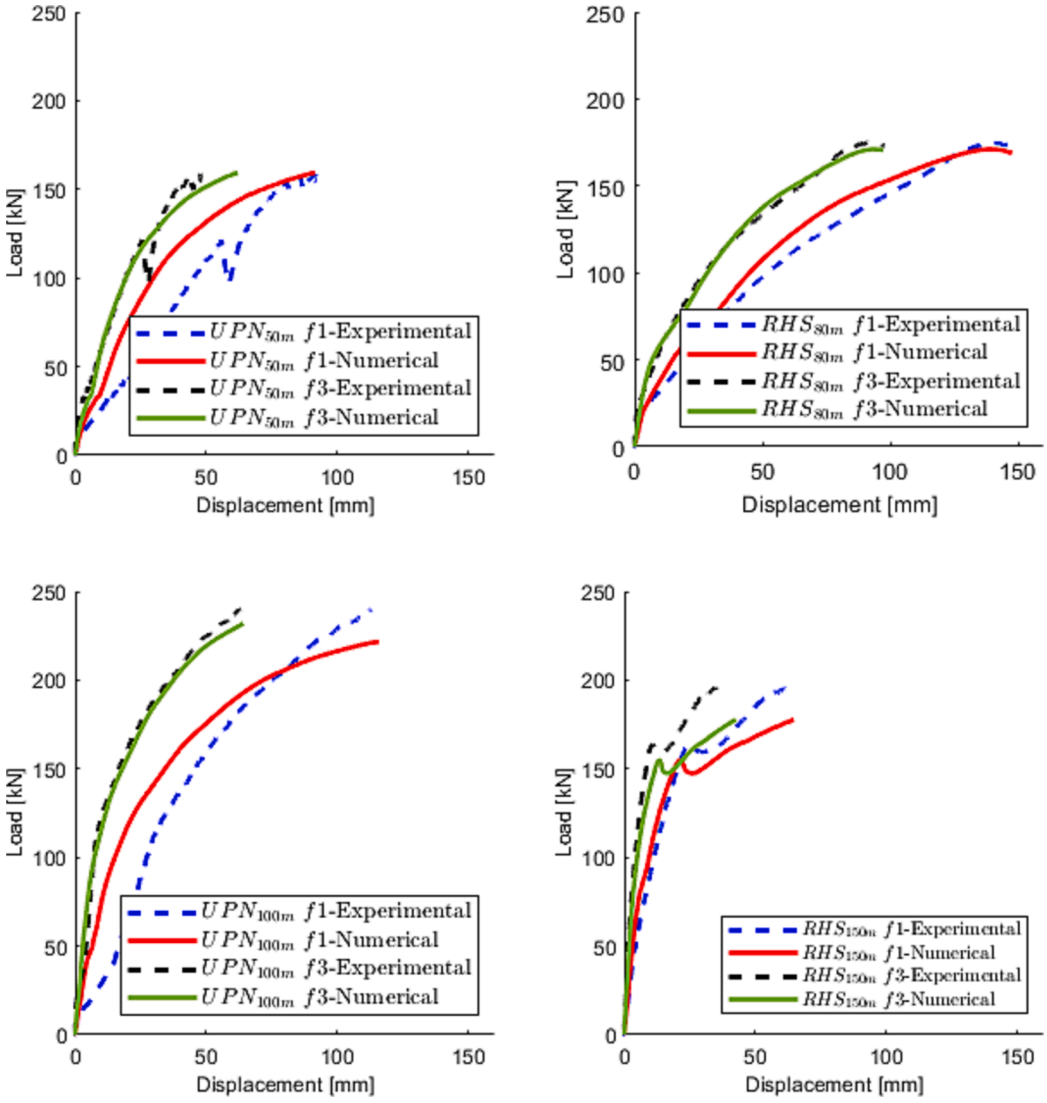

Fig. 11. Experimental vs numerical curves (monotonic load). Tests UPN_{50}, RHS_{80}, UPN_{100}, RHS_{150}.

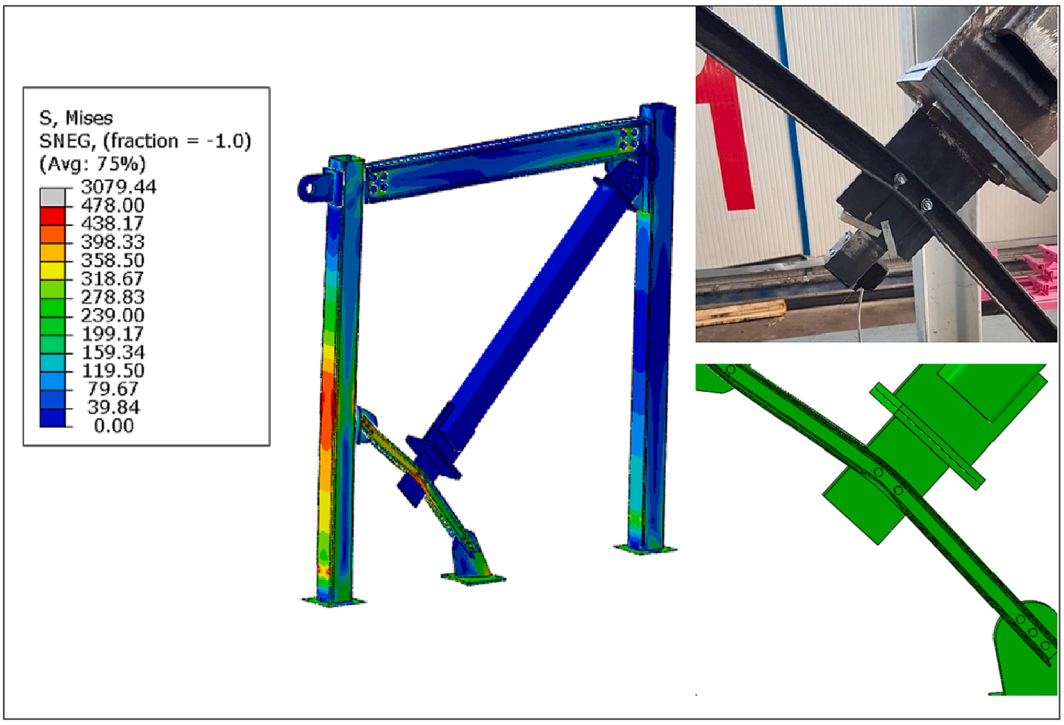

Fig. 12. Specimen UPN_{50m}. Left: Von Mises stress (yield stress of the steel columns 478 MPa - yield stress of the steel fuse 352 MPa). Upper right: last step of the experimental test. Lower right: last step of the numerical analysis.

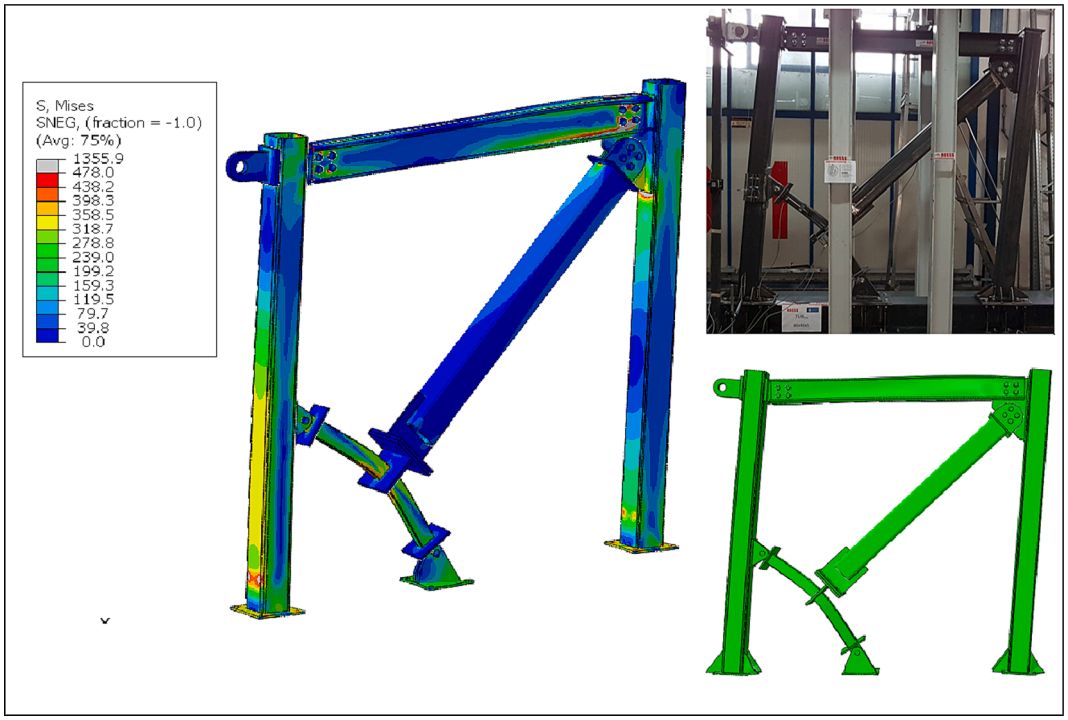

Fig. 13. Specimen RHS_{80m}. Left: Von Mises stress (yield stress of the steel columns 478 MPa - yield stress of the steel fuse 381 MPa). Upper right: last step of the experimental test. Lower right: last step of the numerical analysis.

displacement history is used in all tests: the amplitude of reversed vertical displacements is increased stepwise after the third cycle of each three-cycle series. The cycles have a peak displacement given as a multiple of 10 mm (10 mm, 20 mm, …). Cyclic tests are interrupted at the fuse failure.

3. Results

3.1. Failure mode

The load–displacement (P-f_1) curve is shown in Fig. 5 for all members listed in Table 4. All specimens undergo bending and achieve the

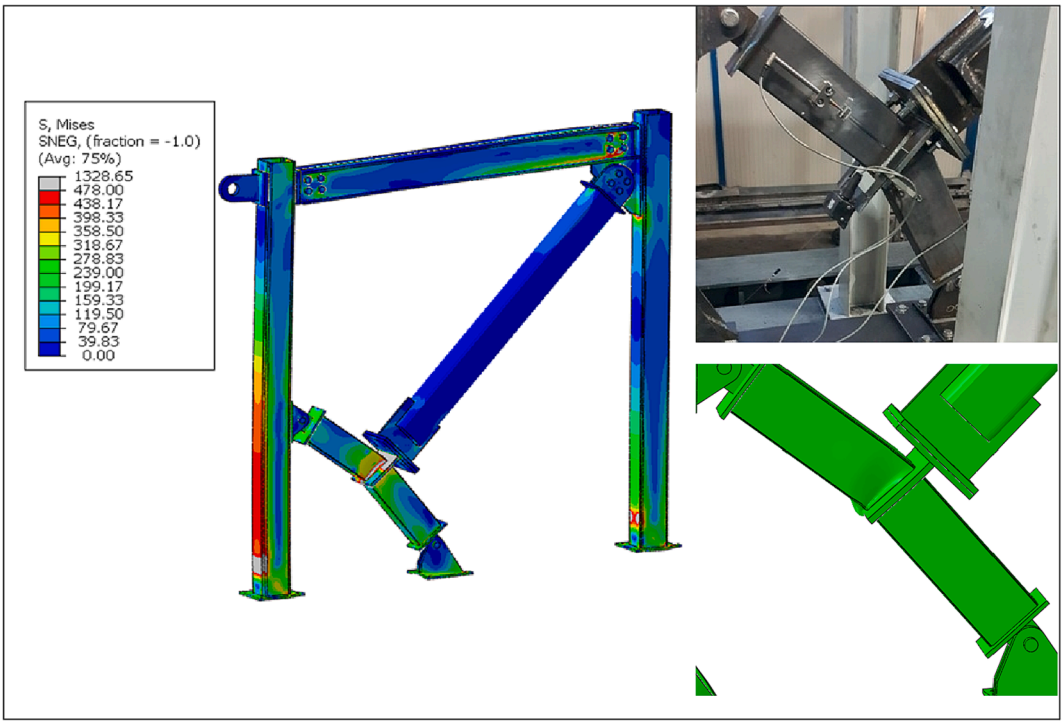

Fig. 14. Specimen RHS_{150m}: Left: Von Mises stress (yield stress of the steel columns 478 MPa - yield stress of the steel fuse 340 MPa). Upper right: last step of the experimental test. Lower right: last step of the numerical analysis.

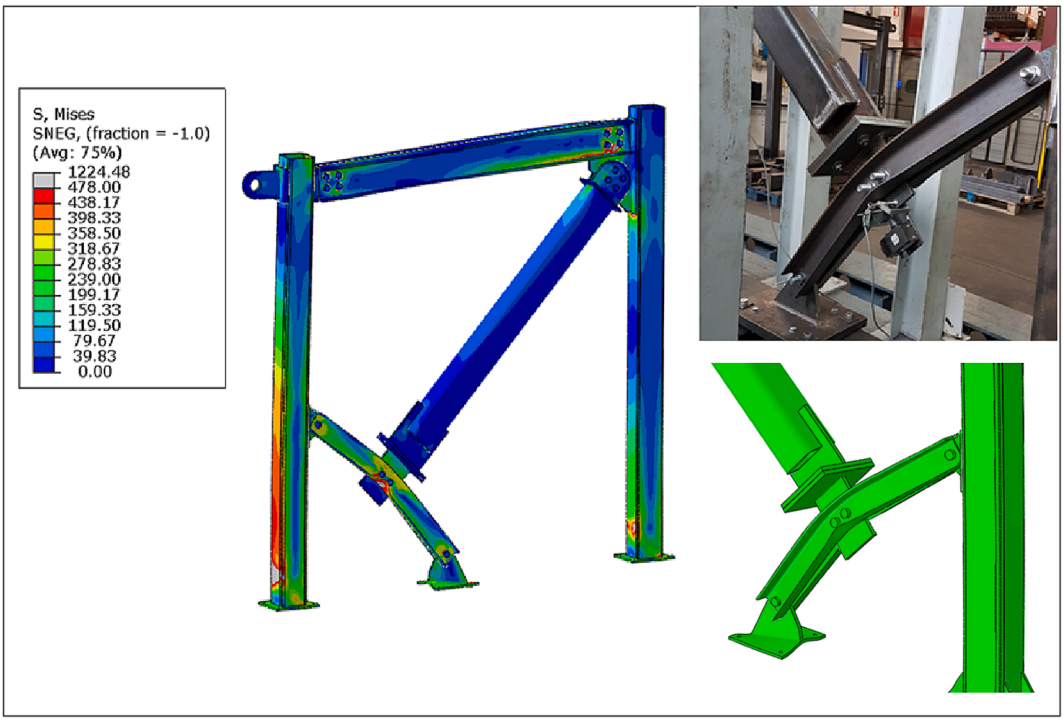

Fig. 15. Specimen $UPN_{100m.}$ Left: Von Mises stress (yield stress of the steel columns 478 MPa - yield stress of the steel fuse 322 MPa). Upper right: last step of the experimental test. Lower right: last step of the numerical analysis.

ultimate moment at the midspan. The failure mode of specimens, related to the ultimate displacement, is listed in Table 5 together with the absolute value of the maximum experimental load P_{max} achieved in cyclic tests. Pictures of some collapse modes observed in experimental tests are shown in Fig. 6.

For specimens with rectangular hollow sections, the failure is due to tearing the flanges after they undergo high deformation due to local buckling at the plastic hinge region (the fuse midspan). For specimens with double-channel sections, the folding of the stiffening lips, caused by local buckling, leads to the tearing of the lips and the failure of the fuse (Fig. 6). As expected, the ultimate load is reached when the fuse midspan section attains its ultimate moment, depending on the plastic section

Table 7
Axial and shear force ratio at the yield moment of the fuse.

	$N/N_{c,\,Rd}$ [-]	$V/V_{pl,\,Rd}$ [-]
UPN_{50m}	0.13	0.15
RHS_{80m}	0.15	0.22
UPN_{100m}	0.05	0.25
RHS_{150m}	0.07	0.40

Table 8
Theoretical vs Numerical yield load.

	Theoretical Yield Load [kN] P_t	Numerical Yield Load [kN] P_n	Ratio [-] P_t/P_n
UPN_{50}	28.4	36.8	0.77
RHS_{80}	30.4	29.6	1.02
UPN_{100}	105.9	102.7	1.03
RHS_{150}	116.0	114.8	1.01

modulus and the steel's ultimate strength.

Suppose a double channel profile is adopted for the fuse. In that case, the critical aspect is represented by global buckling, which can be easily avoided adopting minimum section dimensions and minimum distance between the two channel sections. In contrast, when a RHS is used, the weak component can be represented by the weld between the fuse and the diagonal.

The fuse collapse corresponds to the rotation capacity of the plastic hinge at the fuse midspan. It is worth noting that the same displacement at the top of the frame corresponds to a different distribution of stresses in the structure.

3.2. Dissipated energy

Fig. 7 shows the dissipated energy versus the number of cycles for each specimen. The dissipated energy at the z-th cycle is expressed as: $\sum_{i=1}^{z} E_i$, where E_i is the area inside the i-th hysteresis loop of the force–displacement curve (P-f_1).

In the second and third cycles of each three-cycle series, the energy dissipation capacity undergoes degradation relative to the first cycle. In Fig. 8, the degradation of the dissipated energy is expressed as the percentage ratio of dissipated energy in the second and third cycle to the first cycle within each series (e.g. E_2/E_1 and E_3/E_1 for the first series, E_5/E_4 and E_6/E_4 for the second series, etc.).

Specimens exhibit a uniform trend regardless of the type of the fuse (Fig. 7, Fig. 8). The dissipation of energy per cycle is high such as the stability of the hysteretic loops, the energy dissipation rate in repeating cycles, is near 100 %, greater than tensile diagonals of concentric X bracings ≈ 50 %÷80 % [57,15]. A significant percentage ratio in the first three cycles (E_2/E_1 and $E3/E_1$) is due to the initial slippage phenomenon, nevertheless, it should be observed that the amount of dissipated energy in initial cycles is meager if compared to that of subsequent cycles. Finally, a stable and almost symmetric response depicted by the hysteresis loops of the fuse (Fig. 6), easily replaceable after a seismic event, promotes the use of the proposed dissipative system as a bracing system for earthquake-resistant steel structures designed according to the capacity design approach.

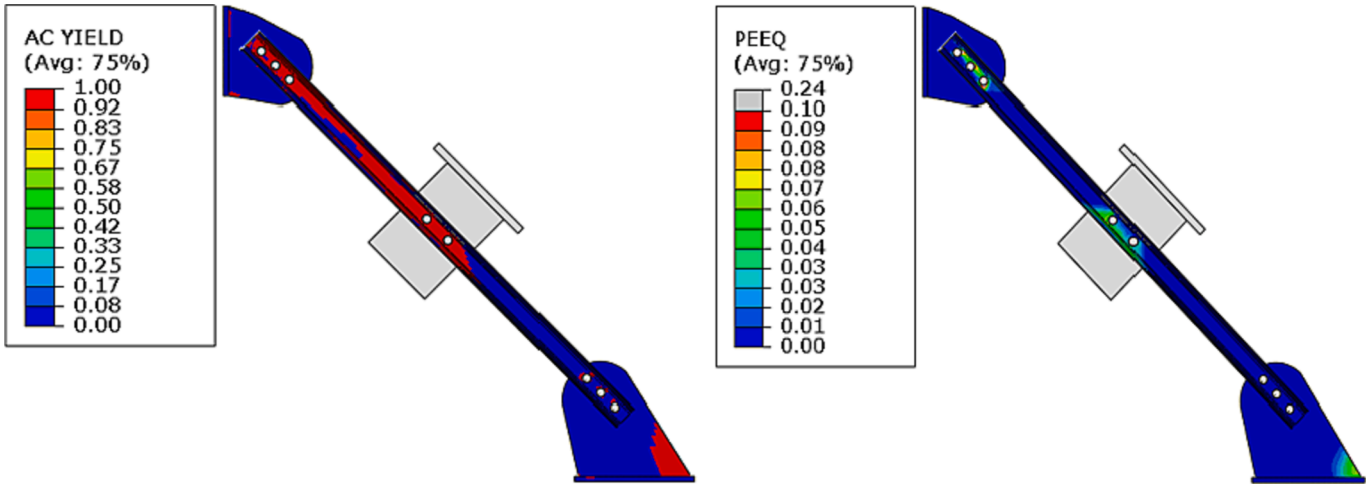

Fig. 16. Fuse plastic deformation for specimen $UPN50_m$.

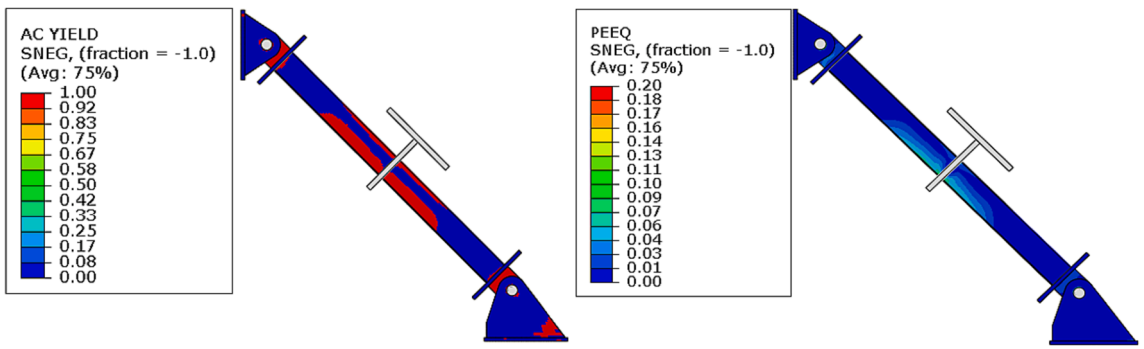

Fig. 17. Fuse plastic deformation for specimen $RHS80_m$.

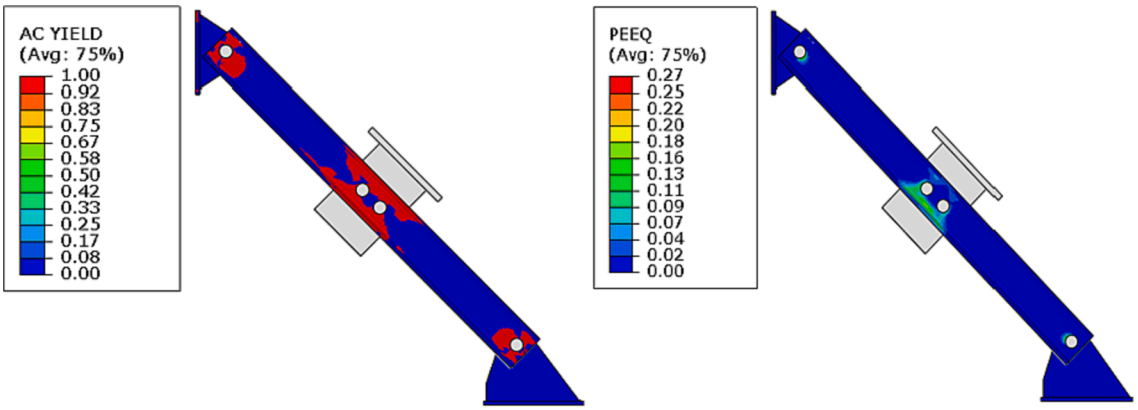

Fig. 18. Fuse plastic deformation for specimen $UPN100_{m.}$

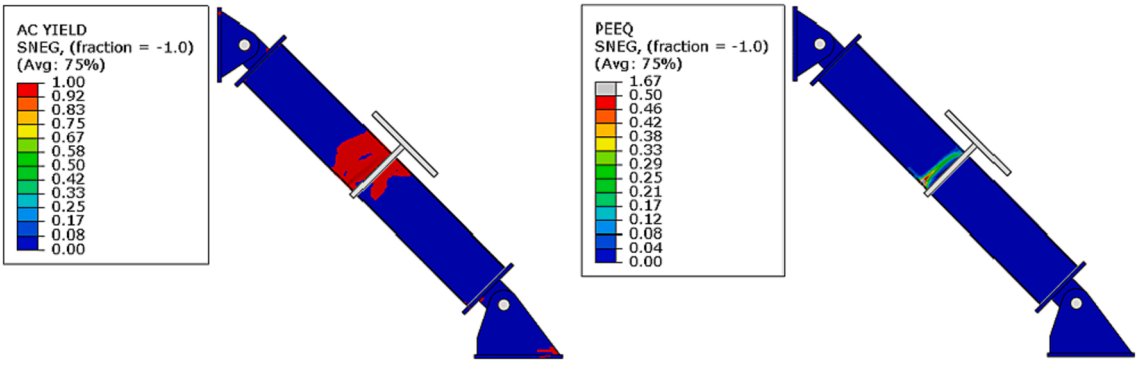

Fig. 19. Fuse plastic deformation for specimen $RHS150_{m.}$

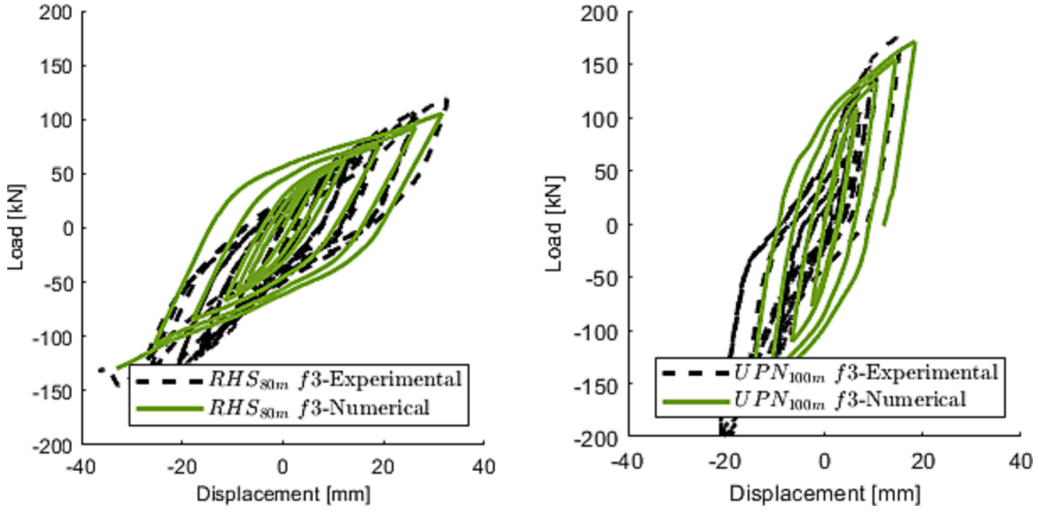

Fig. 20. Experimental vs numerical curves (cyclic load). Tests RHS_{80c}, UPN_{100c}.

4. Numerical simulation

4.1. Mechanical properties

A Finite Element (FE) model is developed in ABAQUS [58] to investigate the structural response of the innovative bracing system. Regarding the mechanical properties, the non-linear hardening stress–strain curve model proposed in [59] is adopted for the steel, exploiting the experimentally estimated yield stress, ultimate stress, and failure elongation (Table 2). Equation (1) reports the constitutive laws according to [59]. For all specimens, the elastic modulus is assumed 210 GPa, and the ultimate elongation is obtained from experimental tests. Fig. 9 displays the constitutive stress–strain curve for all the specimens.

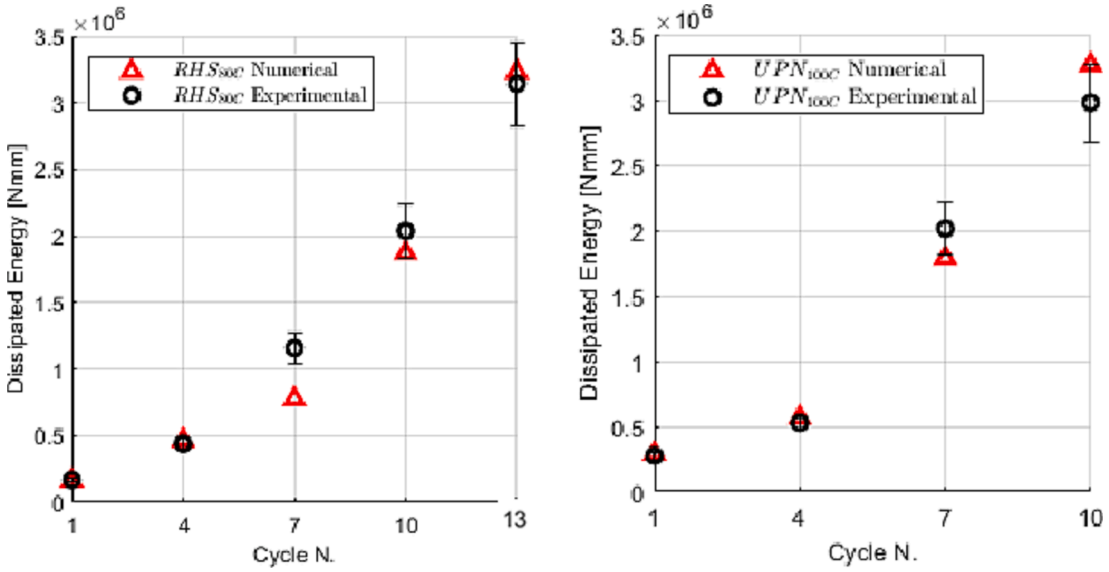

Fig. 21. Comparison of the experimental and numerical dissipated energy (bars represent ±10 % difference from experimental data).

Table 9
The seismic behavior factor of the proposed bracing system for different fuses.

Specimen	q-factor
UPN_{50}	2.53
RHS_{80}	2.95
UPN_{100}	3.35
RHS_{150}	3.05

$$f(\varepsilon)=\begin{cases} E\varepsilon \quad \text{for} \quad \varepsilon<\varepsilon_y \\ f_y \quad \text{for} \quad \varepsilon_y<\varepsilon\le\varepsilon_{sh} \\ f_y+(f_u-f_y)\left\{0.4\left(\dfrac{\varepsilon-\varepsilon_{sh}}{\varepsilon_u-\varepsilon_{sh}}\right)+\dfrac{2\left(\dfrac{\varepsilon-\varepsilon_{sh}}{\varepsilon_u-\varepsilon_{sh}}\right)}{\left[1+400\left(\dfrac{\varepsilon-\varepsilon_{sh}}{\varepsilon_u-\varepsilon_{sh}}\right)^5\right]^{\frac{1}{5}}}\right\} \text{ for } \varepsilon_{sh}<\varepsilon\le\varepsilon_u \end{cases} \tag{1}$$

where E is the elastic modulus, f_y is the yield stress, ε_y is the yield strain, f_u is the ultimate stress and $\varepsilon_{sh}=0.1f_y/f_u-0.055$.

A combined isotropic-kinematic model [58] simulates the cyclic response with the parameters proposed in [60] and listed in Table 6.

4.2. Finite element modeling

The columns (RHS 150x150x10), the two portal beams (2xUPN160), and the long diagonal (RHS 150x150x10) are modeled with both bidimensional and tridimensional elements: shell type S4R and S3 are adopted for the frame columns, the diagonal and RHS fuses; solid type C3D8R is adopted for the plates, UPN160, bolts, and UPN fuses. Mesh sizes depend on the element: 12 mm for columns and portal beams, 10 mm for plates, and 3 mm for bolts and fuses. Moreover, the mesh is refined for solid elements to use only hexahedral elements and avoid tetrahedral ones for better precision and fewer degrees of freedom. Bolts are modeled according to the actual geometry, with pre-load and surface-to-surface contacts. Contact properties are the following: penalty formulation with a friction coefficient of 0.2 in the tangential direction and "Hard" contact in normal behavior [58]. All the welds are simulated using tie constraints. Base plates are connected to the ground using appropriate linear connectors to reproduce the flexibility of the testing apparatus measured in experimental tests. Monotonic and cyclic tests were carried out using both geometric and material nonlinearities. The type of analysis is "static," and it is divided into two steps: a "pre-load step" where only the bolt load is applied, and a "displacement control step." The model is displayed in Fig. 10.

4.3. Numerical results

4.3.1. Monotonic tests

Fig. 11 reports the capacity curve (P-f_1 and P-f_3) for RHS_{80m}, UPN_{50m}, RHS_{150m}, and UPN_{100m}, respectively; where P is the external load applied at the top of the portal frame, f_1 is the horizontal displacement at the control point (where the external load is applied) and f_3 the displacement at the fuse mid-span along the long diagonal axis (Fig. 2).

Numerical curves fit the experimental ones confirming the accuracy of the FE model. A change in the slope of the load–displacement curve in the RHS_{150} specimen is due to the fuse failure because of local buckling of the compressed flange, after that the ultimate moment is achieved. Nevertheless, the external load can increase because of the resistance provided by the portal frame.

The numerical model is adopted to estimate the stress distribution on members at the fuse failure. Von Mises stresses are plotted in Figs. 12-15, where the upper limit of the legend (478 MPa) refers to the experimental

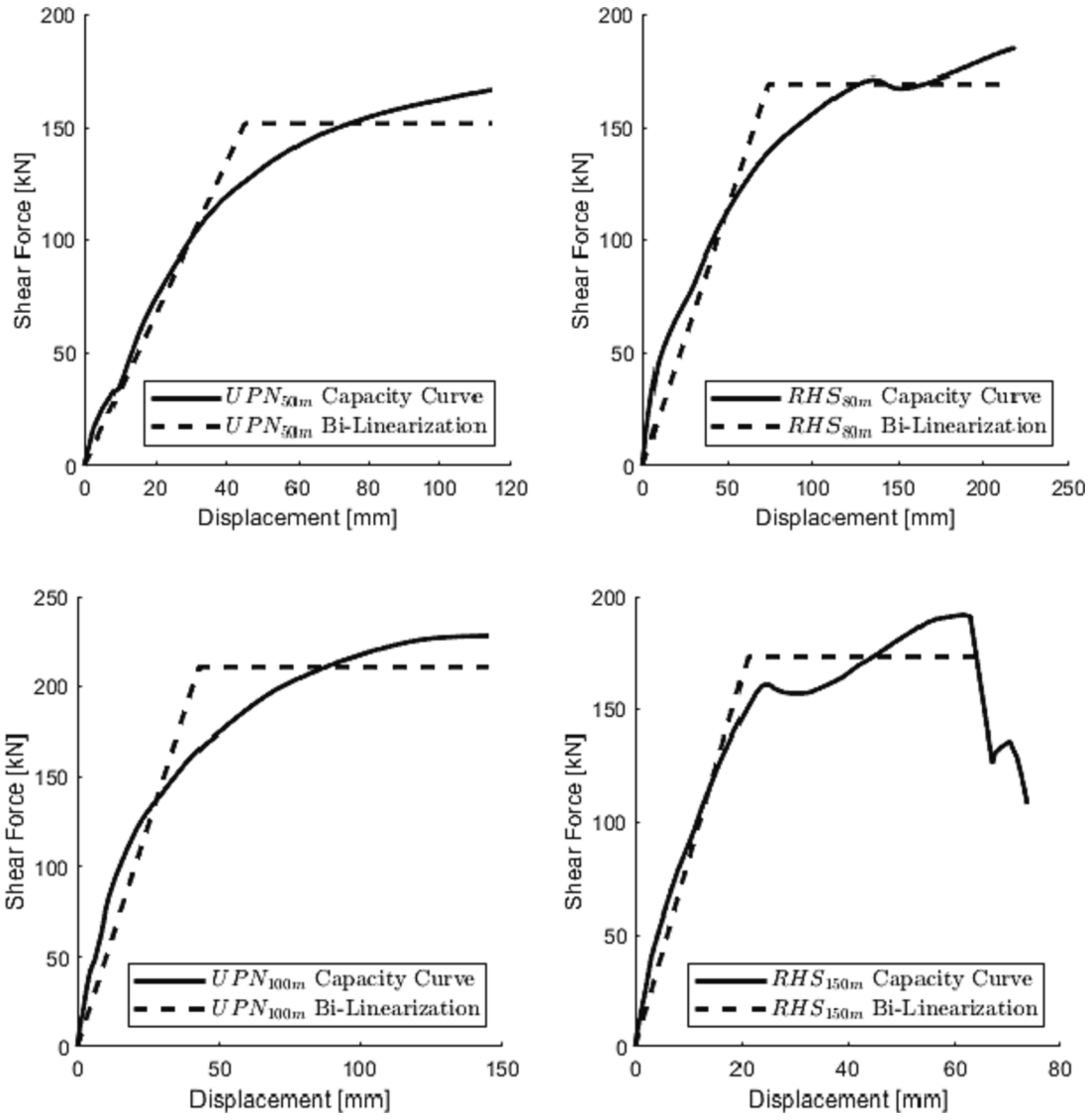

Fig. 22. Capacity curves and corresponding bi-linearization.

yield stress of the columns. Results confirm that the portal frame members remain in the elastic field and have the capacity to replace the system close to the initial configuration after the fuse failure for its easy replacement.

Numerical simulations clearly show that in all tests, the fuses reach the yield moment M_y at midspan, then large strains develop in the plastic field.

The fuses are also subject to axial and shear forces, nevertheless, their influence on the yield moment is negligible. The ratio between the effective axial and shear forces ($N - V$) and the resistant axial and shear force ($N_{c,\ Rd}$ - $V_{pl,\ Rd}$) at the yield moment are listed in Table 7.

A maximum ratio of 40 % for the shear force (<50 % [53,61,62]) and 15 % for the axial force (<20 % [53,61,62]) proves the influence of the axial and shear forces on the fuse bending capacity be actually negligible.

The fuses' flexural response is confirmed by comparing the yield theoretical load evaluated on a simply supported beam under a three-point bending load and the FE numerical yield load transferred by the long diagonal to the fuse at the formation of the plastic hinge (Table 8). Theoretical results agree with the numerical ones; the greater difference affects the UPN50 (0.77) and is mainly due to the use of three bolts connecting the fuse to the frame, which modifies the static scheme by introducing elastic rotational restraints at both ends.

Fig. 16, Fig. 17, Fig. 18, and Fig. 19 display the plastic region (AC YIELD) and the Equivalent Plastic Strain (PEEQ).

The magnitude of the fuses' strains allows the identification of the plastic hinge length. The smaller ratio between the ultimate and yield moment in RHS_{150} ($f_yW_{p,xx}/f_yW_{e,xx}$) reflects a limited plastic hinge length (Fig. 19). Consequently, using three bolts connecting the fuse to the frame, which transfers the bending moment, modifies the stress distribution in the UPN_{50}, as highlighted by the plastic deformation achieved at the compressed flange close to the fuse end. The asymmetrical strain distribution results from a different stiffness between the portal frame-fuse joint and the fuse-base joint. Using a single bolt to join the fuse to the portal frame is recommended to reduce connection damage and facilitate the replacement of the fuse.

4.3.2. *Cyclic tests*

The experimental and numerical cyclic load–displacement curve (P-f_3) are shown in Fig. 20 for specimens RHS_{80c} and $UPN_{100c,}$ respectively.

Numerical curves well fit the experimental ones; a slight slippage phenomenon in experimental curves is due to the yielding of the column baseplates, whose deformation has been neglected in the numerical simulation to reduce computation time.

The dissipated energy relative to every single cycle obtained from the experimental test and the numerical model is shown in Fig. 21, where the error bars refer to a ±10 % from the experimental data. The dissipated energy is the mean obtained in cycles with the same displacement.

The remarkable stability and symmetry of the hysteresis loops promote the use of the proposed system as a dissipative member in earthquake-resistant steel structures designed according to the capacity requirements.

5. Q-Factor Estimation

The seismic behavior factor ("q-factor") estimation is made considering monotonic tests and the well-known equal displacement rule [63].

Experimental tests, interrupted at the fuse failure, are numerically extended using the FE model presented in §4 for a reliable estimation of the overall system (portal frame plus fuse). Since the idea behind this dissipative bracing system is that the fuse is the only element to undergo plastic deformation, the numerical analyses stop criterion is linked to the yield point of the columns of the frame. The q-factors are listed in Table 9 for all investigated specimens, and Fig. 22 shows the capacity curve and relative bilinearization.

6. Concluding remarks

The paper presents the results of an experimental campaign of an innovative steel bracing system formed by a portal frame with hinged joints connected through a diagonal to a fuse. The portal frame remains in the elastic field and could provide the energy to relocate the system after an earthquake; the dissipation of energy is provided by the fuse, which behaves like a beam in three-point bending, and its cross-section can be designed to prevent out-of-plane instability; the use of a single bolt to join the fuse and the portal frame allows an easy replacement of the fuse. A reliable FE numerical model is developed to estimate the impact of structural details and design parameters on the bracing response and evaluate the seismic behavior factor.

The main results can be summarized as follows:

1. The proposed bracing system provides excellent stability and symmetric response in the hysteresis loops meaning that it is fully capable of dissipating energy during an earthquake;
2. Fuse double C-sections have better behavior than rectangular hollow sections with the same elastic section modulus, as rectangular hollow sections can undergo local buckling thus exhibiting lower rotation ductility;
3. Behavior factors of tested fuse cross-sections vary from 2.53 to 3.35, depending on the profile;
4. For multilevel buildings, the proposed system allows to efficiently satisfy the limitations on the overstrength coefficient at all storeys by simply changing the fuse cross-section and/or its length;
5. The system is easily replaceable after a seismic event, with an affordable replacement cost.

CRediT authorship contribution statement

Alessandro Mei: Methodology, Formal analysis, Data curation, Writing – original draft, Writing – review & editing, Visualization. **Federico Gusella:** Methodology, Investigation, Data curation, Writing – original draft, Writing – review & editing, Visualization. **Maurizio Orlando:** Conceptualization, Methodology, Writing – original draft, Writing – review & editing, Supervision, Project administration, Funding acquisition.

Declaration of Competing Interest

The authors declare that they have no known competing financial interests or personal relationships that could have appeared to influence the work reported in this paper.

Data availability

The data that has been used is confidential.

Acknowledgments

The authors gratefully acknowledge the Italian Rack Manufacturing Company ROSSS SpA, Scarperia and San Piero, Florence (IT), especially the President Stefano Bettini, for hosting the experimental set-up. The study is part of the Research Program SmartISS "Smart Industrial Steel Structures", developed under the scientific supervision of M. Orlando, with the financial support of Tuscany Region within the Regional Operational Programme POR CreO FESR 2014-2020 (Lines of Action 1.1.4 and 1.1.5, Call for Proposals R & D, 2017).

References

[1] Eurocode 8 – Design of structures for earthquake resistance – Part. 1: General rules, seismic actions and rules for buildings. EN 1998-1:2004.
[2] Gusella F, Orlando M, Peterman KD. On the required ductility in beams and connections to allow a redistribution of moments in steel frame structures. Eng Struct 2019;179:595–610.
[3] Gusella F, Orlando M, Spinelli P. Pinching in Steel Rack Joints: Numerical Modelling and Effects on Structural Response. International Journal of Steel Structures 2019;19(1).
[4] Yin L, Tang G, Li Z, Zhang M. Responses of cold-formed steel storage racks with spine bracings using speed-lock connections with bolts II: Non-linear dynamic response history analysis. Thin-Walled Struct 2018;125:89–99.
[5] Yin L, Tang G, Li Z, Zhang M, Feng B. Responses of cold-formed steel storage racks with spine bracings using speed-lock connections with bolts I: Static elastic-plastic pushover analysis. Thin-Walled Struct 2018;125:51–62.
[6] Leng J, Peterman KD, Bian G, Buonopane SG, Schafer BW. Modeling seismic response of a full-scale cold-formed steel-framed building. Eng Struct 2017;153:146–65.
[7] Mei A, Orlando M, Salvatori L, Spinelli P. Nonlinear Static And Incremental Dynamic Analyses For Seismic Down-Aisle Behavior Of Rack Structures | Analisi Statiche Non Lineari E Dinamiche Incrementali Per La Caratterizzazione Sismica In Direzione Longitudinale Di Scaffalature Portapallet. Ingegneria Sismica 2021;38(2):21–45.
[8] S. Movaghati, A.E. Abdelnaby. Experimental study on the non-linear behavior of bearing-type semi-rigid connections (2019). Engineering Structures, 199 109609.
[9] Gusella F, Arwade SR, Orlando M, Peterman KD. Influence of mechanical and geometric uncertainty on rack connection structural response. Journal of Constructional Steel ResearchVolume February 2019;153:343–55.
[10] Padilla-Llano DA, Moen CD, Eatherton MR. Cyclic axial response and energy dissipation of cold-formed steel framing members. Thin-Walled Struct 2014;78:95–107.
[11] Goggins JM, Broderick BM, Elghazouli AY, Lucas AS. Experimental cyclic response of cold-formed hollow steel bracing members. Eng Struct 2005;27:977–89.
[12] Moen CD, Schafer Bw. Experiments on cold-formed steel columns with holes. Thin-Walled Struct 2008;46(10):1164–82.
[13] Pu Y, Godley MHR, Beale RG, Lau HH. Prediction of Ultimate Capacity of Perforated Lipped Channels. J Struct Eng 1999;125(5):510–4.
[14] Legeron F, Desjardins E, Ahmed E. Fuse performance on bracing of concentrically steel braced frames under cyclic loading. J Constr Steel Res 2014;95:242–55.
[15] Gusella F, Lavacchini G, Orlando M, Spinelli P. Axial response of cold-formed steel bracing members with holes. J Constr Steel Res 2019;161:70–85.
[16] Orlando, M., Lavacchini, G., Ortolani, B., Spinelli, P. Experimental capacity of perforated cold-formed steel open sections under compression and bending, Steel and Composite Structures, Volume 24, Issue 2, Pages 201 – 211; 10 June 2017.
[17] Vincenzo Macillo, Ornella Iuorio, Maria Teresa Terracciano, Luigi Fiorino, Raffaele Landolfo. Seismic response of CFS strap-braced stud walls: Theoretical study, Thin-Walled Structures, 85 (2014) 301–312.
[18] Luigi Fiorino, Maria Teresa Terracciano, Raffaele Landolfo. Experimental investigation of seismic behaviour of low dissipative CFS strap-braced stud walls, Journal of Constructional Steel Research, 127 (2016) 92–107.
[19] Fiorino L, Shakeel S, Macillo V, Landolfo R. Seismic response of CFS shear walls sheathed with nailed gypsum panels: Numerical modelling. Thin-Walled Struct 2018;122:359–70.
[20] Zampieri P, Curtarello A, Maiorana E, Pellegrino C. A Review of the Fatigue Strength of Shear Bolted Connections. International Journal of Steel Structures 2019;19(4):1084–98.
[21] O. C. Celik, J. W. Berman, M. Bruneau (2004), Cyclic Testing of braces Laterally Restrained by Steel Studs to Enhance Performance During Earthquakes. Technical Report MCEER-04-0003.
[22] Tremblay R. Inelastic seismic response of steel bracing members. J Constr Steel Res 2002;58:665–701.

[23] R. Gary Black, W. A. Bill Wenger, Egor P. Popov. Inelastic buckling of steel struts under cyclic load reversals. Report to Sponsors: National Science Foundation, American Iron and Steel Institute, October (1980).
[24] Nip KH, Gardner L, Elghazouli AY. Cyclic testing and numerical modelling of carbon steel and stainless steel tubular bracing members. Eng Struct 2010;32:424–41.
[25] Mashhadiali, N., Saadati, S., Mohajerani, S.A.M., Ebadi, P. Hybrid braced frame with buckling-restrained and strong braces to mitigate soft story (2021) Journal of Constructional Steel Research, 181, art. no. 106610.
[26] Nejati, F., Zhian, M., Safar Mashaie, F., Edalatpanah, S.A. Computational modeling of yielding octagonal connection for concentrically braced frames (2020) Magazine of Civil Engineering, 94 (2), pp. 31-53.
[27] Zheng, L., Wang, W., Dou, S., Ge, H., Gao, Y., Han, Y. Seismic performance of braced frame structure with double-cylinder arc energy dissipator (2022) Thin-Walled Structures, 180, art. no. 109950.
[28] Thongchom, C., Mirzai, N.M., Chang, B., Ghamari, A. Improving the CBF brace's behavior using I-shaped dampers, numerical and experimental study (2022) Journal of Constructional Steel Research, 197, art. no. 107482.
[29] Ghamari, A., Kim, Y.-J., Bae, J. Utilizing an I-shaped shear link as a damper to improve the behaviour of a concentrically braced frame (2021) Journal of Constructional Steel Research, 186, art. no. 106915.
[30] Ghamari, A., Haeri, H., Khaloo, A., Zhu, Z. Improving the hysteretic behavior of Concentrically Braced Frame (CBF) by a proposed shear damper (2019) Steel and Composite Structures, 30 (4), pp. 383-392.
[31] Mohsenzadeh, V., Wiebe, L. Replaceable Brace Modules for Concentrically Braced Frames: Test Results from Substructure with Moment-Resisting Beam-Column Connections (2022) Lecture Notes in Civil Engineering, 262 LNCE, pp. 844-851.
[32] Paronesso, M., Lignos, D.G. Seismic design and performance of steel concentrically braced frame buildings with dissipative floor connectors (2022) Earthquake Engineering and Structural Dynamics, 1-21.
[33] Henriques, J., Calado, L., Castiglioni, C.A., Degée, H. Dissipative connections with U-shaped steel plate for braces of concentrically braced frames (2019) Bulletin of Earthquake Engineering, 17 (11), pp. 6203-6237.
[34] Faytarouni M, Seker O, Akbas B, Shen J. Seismic assessment of ductile concentrically braced frames with HSS bracings. Eng Struct 2019;191:401–16.
[35] Kumar PCA, Sahoo DR, Kumar A. Seismic response of concentrically braced frames with staggered braces in split-x configurations. J Constr Steel Res 2018;142:17–30.
[36] Seker O, Faytarouni M, Akbas B, Shen J. A novel performance-enhancing technique for concentrically braced frames incorporating square HSS. Eng Struct 2019;201.
[37] Morrison, M.L. A ductile fuse for special concentrically braced frames (2020) Proceedings of the 9th International Conference on Advances in Steel Structures, ICASS 2018.
[38] Mirzai, N.M., Cho, H.M., Hu, J.W. Experimental study of new axial recentering dampers equipped with shape memory alloy plates (2021) Structural Control and Health Monitoring, 28 (3), art. no. e2680.
[39] Marzok, A., Lavan, O. Optimization Based Seismic Design of Self-centering Concentrically Braced Frames (2022) Lecture Notes in Civil Engineering, 262 LNCE, pp. 737-745.
[40] Tian, L., Qiu, C. Modal pushover analysis of self-centering concentrically braced frames (2018) Structural Engineering and Mechanics, 65 (3), pp. 251-261.
[41] Giugliano MT, Longo A, Montuori R, Piluso V. Plastic design of CB-frames with reduced section solution for bracing members. J Constr Steel Res 2010;66(5):611–21.
[42] Dario Aristizabal-Ochoa J. Disposable Knee bracing: Improvement in seismic design of steel frames. J Struct Engineering, ASCE 1986;112:1544–52.
[43] Balendra, T., Sam, M.-T., Liaw, C.-Y., Lee, S.-L. Preliminary studies into the behaviour of knee braced frames subject to seismic loading (1991) Engineering Structures, 13 (1), pp. 67-74.
[44] Balendra, T., Lim, E.-L., Lee, S.-L. Ductile knee braced frames with shear yielding knee for seismic resistant structures (1994) Engineering Structures, 16 (4), pp. 263-269.
[45] Yahyapour, R., Seyedpoor, S.M. Comparing the Seismic Behavior of Various Knee Braced Steel Frames Based on Incremental Dynamic Analysis and Development of Fragility Curves (2021) International Journal of Steel Structures, 21 (4), pp. 1228-1241.
[46] Sheidaii, M.R., TahamouliRoudsari, M., Gordini, M. Investigation of the non-linear seismic behavior of knee braced frames using the incremental dynamic analysis method (2016) International Journal of Advanced Structural Engineering, 8 (2), pp. 151-159.
[47] Jafari, V., Akbarpour, A. Effect of near-field earthquake excitation on seismic behavior of knee-braced moment frames (2018) Asian Journal of Civil Engineering.
[48] Bourahla, N., Blakeborough, A. Similitude distortion compensation for a small scale model of a knee braced steel frame (2015) American Journal of Engineering and Applied Sciences, 8 (4), pp. 481-488.
[49] Ghafouri-Nejad A, Alirezaei M, Mirhosseini SM, Zeighami E. Parametric study on seismic response of the knee braced frame with friction damper. Structures 2021;32:2073–87.
[50] Zahrai, S.M., Jalali, M. Experimental and analytical investigations on seismic behavior of ductile steel Knee Braced Frames (2014) Steel and Composite Structures, 16 (1), pp. 1-21.
[51] FEMA 365 (2000). Prestandard and commentary for the seismic rehabilitation of buildings. ASCE American Society of Civil Engineers.
[52] Bruneau, M., Uang C.M., Sabelli, R. Ductile design of steel structures. 2nd Edition, McGraw Hill ISBN: 978-0071623957.
[53] Eurocode 3 - Design of steel structures- Part. 1-1: General rules and rules for buildings. EN 1993-1-1, 2005.
[54] Gusella F, Orlando M. Analysis of the Dissipative Behavior of Steel Beams for Braces in Three-Point Bending. Eng Struct 2021;244.
[55] International Standard ISO 6892-1:2009. Metallic materials – Tensile testing Part1: Method of test at room temperature.
[56] ATC-24 (1992), Guidelines for cyclic seismic testing of components of steel structures.
[57] Bruneau, M., Uang C.M., Sabelli, R. Ductile design of steel structures. 2nd ed., McGraw Hill (ISBN: 978-0071623957).
[58] Abaqus. Analysis User's Manual. Dassault Systémes Simulia Corp; 2020.
[59] Yun X, Gardner L. Stress-Strain Curves for Hot-Rolled Steels. J Constr Steel Res 2017;133:36–46.
[60] Hartloper, Alexander R., Albano de Castro e Sousa, and Dimitrios G. Lignos. "Constitutive Modeling of Structural Steels: Non-linear Isotropic/Kinematic Hardening Material Model and Its Calibration." Journal of Structural Engineering 147, no. 4 (2021): 1–17.
[61] Goczek J, Supeł Ł. Resistance of steel cross-sections subjected to bending, shear and axial forces. Eng Struct 2014;70:271–7. https://doi.org/10.1016/j.engstruct.2014.02.016.
[62] Gusella, F., Orlando., M., K. D. Peterman, The impact of variability and combined loads on fuses in braced frames, Structures, Volume 35, January 2022, 650-666.
[63] Chopra AK. Dynamics of Structures. Prentice Hall - Pearson: Fourth Edition; 2012.